# Molecular dynamics approach for the calculation of the surface loss probabilities of neutral species in argon-methane plasma

Glenn-christopher Otakandza-Kandjani, Pascal Brault, Maxime Mikikian, Armelle Michau, Khaled Hassouni

*RESEARCH ARTICLE*

# *Molecular dynamics approach for the calculation of the surface loss probabilities of neutral species in argon-methane plasma*

Glenn Otakandza Kandjani[1] | Pascal Brault[1*] | Maxime Mikikian[1] | Armelle Michau[2] | Khaled Hassouni[2]

[1] *GREMI, UMR7344, CNRS/Université d'Orléans, F-45067, Orléans Cedex 2, France*

[2] *LSPM, UPR3407, CNRS/Université Sorbonne Paris Nord, F-93430, Villetaneuse, France*

**Correspondence*

*Pascal Brault, GREMI, CNRS, Université d'Orléans, 45067 Orléans Cedex 2, France.*

*Email: pascal.brault@univ-orleans.fr*

***Abstract***

Molecular dynamics simulations are carried out for calculating the surface loss probabilities of neutral species from an argon-methane plasma. These probabilities are the sum of the sticking and surface recombination probabilities. This study considers both the formation of reactive and nonreactive volatile species for evaluating recombination probabilities. Results show that stable species are reflected when hydrocarbon film starts growing on the surface. $CH_3$ is mainly lost by surface recombination leading to formation of volatile products while very little contributes to film growth. $C_2H$ has surface loss probability in agreement with literature. While $C_2H$ loss is usually attributed to sticking on the surface, our results show that its main loss process is due to surface recombination.

***Keywords****: molecular dynamics, sticking probability, surface recombination probability, surface loss probability, hydrocarbon plasma, C:H film*

## 1 INTRODUCTION

Low-temperature hydrocarbon plasmas are weakly ionized gases, containing a variety of different species (electrons, ions, neutrals, radicals, etc).[1]–[3] These plasmas are an important tool for the fabrication of materials such as carbon nanotubes, nanowalls, and other advanced carbon nanostructures. [4], [5] These materials have a wide range of applications, such as composite materials for construction, drug delivery, energy storage and conversion, etc. [6], [7]. These plasmas are also used to deposit thin films of diamond and diamond-like carbon (DLC) [8], [9], commonly used for their infrared transparency or as hard coatings for tools and optical devices. [10]–[12] However, despite this interest, the complexity of the chemical reactions that take place in these plasmas makes their understanding and control quite difficult, since they are governed by reactions occurring both in the volume and on the surrounding surfaces. Surface reactions can significantly affect the plasma phase chemistry. These reactions depend on the surface properties (e.g. materials, structure, density of dangling bonds), and on the energy and nature of the incoming particles interacting with the surface.[13] The sticking probability is a key parameter that provides information about the contribution of the plasma species to the growth of films on the surface. [14]The calculation of the sticking probabilities is based on empirical approaches and their values can sometimes be very rough approximations, since their experimental measurements are relatively complex.[15], [16]

The sticking probabilities are often estimated to be zero for non-radical neutral species, since they are not expected to contribute to film growth. [13], [17], [18] Thus, the growth of a hydrocarbon (C:H) film on the surface results from radicals and ions impinging on the surface. The sticking probabilities of ions impinging on the surface are assumed to be close to one and are determined by numerical simulations.[15], [19], [20]

To calculate the sticking probability for radical neutral species, one approach is to measure the "surface loss probability (β)" also named "surface reaction probability."[15], [16] In these works, this probability is defined as the sum of the sticking probability and the probability that the species reacts via surface reactions to form a non-reactive volatile product (also called surface recombination probability). [13], [15], [16] Therefore, this surface loss probability, which is equal to the upper limit of the sticking probability, is at present used to estimate the sticking probability of various hydrocarbon radicals.[15]

Hopf et al[15] experimentally measured the surface loss probabilities of various hydrocarbon radicals during growth of amorphous hydrogenated carbon films (a-C:H, with H to C ratio greater than or equal to 1, i.e. soft films) . Based on the spatial variation of the thickness of the a-C:H film (deposition profile), the authors derived the surface loss probability and then

estimated the sticking probability. They found that the surface loss probability of the $C_2H$ radical was about 0.9 in acetylene-based plasmas and 0.8 in other hydrocarbon plasmas. Using these values, the authors were able to determine the sticking probability by estimating the surface recombination probability. For the $CH_3$ radical, its surface loss probability is estimated to be less than 0.01 and may change depending on the plasma conditions.[16]

The question that we wish to address in our study is to calculate independently sticking and surface recombination probabilities of the species during the growth of C:H films in argon-methane plasmas by atomistic methods, taking into account the formation of both reactive (usually not considered) and non-reactive volatile products.

Molecular dynamics (MD) simulations have been widely used to calculate sticking probability (S), and reflection probability (r) of gas species interacting with a surface. [21]–[27] Knowledge of the reflection probability, allows to deduce the surface loss probability β, since $r = 1 - \beta$.[13] For example, Sharma et al. [24] performed MD simulations to determine the reflection probabilities of hydrocarbon molecules and radicals on an a-C:H surface. The authors observed that these reflection probabilities decreased with increasing incident energy of the radical, leading to an increase in the surface loss. On the other hand, the authors observed that at low energies (up to 0.75 eV) stable hydrocarbon species (neutral, non-radical species) had a reflection probability of 100% (i.e. no loss at the surface) and that hydrocarbon radicals with fewer hydrogen atoms had high surface loss probabilities compared to those with more hydrogen atoms.

Alman et Ruzic [25] studied the reflection probabilities of hydrocarbon radicals on a "soft" and "hard" carbon surface using MD simulations. The "soft" surface was a layer of a-C:H redeposited on a graphite surface, and the "hard" surface was a graphite network bombarded with hydrogen. The authors found that the surface loss probabilities of hydrocarbon radicals were higher on the soft surface than on the hard surface. And as for the stable neutral species, the authors found that regardless of the type of surface, they were completely reflected at low energy and underwent fragmentation at high energy (from about 2 eV).

Molecular dynamics simulations are therefore relevant to determine either the sticking probability or the reflection probability of a species. To our knowledge, these methods have not yet been used to distinguish losses due sticking from those due to surface recombination.

Therefore, the goal of our study is to determine the surface loss probabilities of the major neutral species ($H_2$, $CH_4$, $C_2H_4$, $C_2H$, $C_2H_2$, and $CH_3$, excluding Ar) of an argon-methane plasma at room temperature (300 K) using molecular dynamics simulations. These surface loss probabilities are calculated by determining the sticking and surface recombination probabilities

(taking into account non-reactive and reactive volatiles) of each of these species during the growth of a C:H film on a stainless steel surface. These initial neutral species interacting with the surface are obtained from a 1D kinetic model of a low-pressure Ar / 4% $CH_4$ plasma created by a radiofrequency discharge.[28]–[30]

This paper is organized as follows: In the next section, we present the methodology and computational details. In Section 3, we first present the sticking probabilities of each neutral species on two types of surfaces: a pristine surface and a surface covered with a C:H film. In section 4, we discuss the surface loss probabilities of these same species during the growth of the C:H film and we present a mass spectrum of the formed volatile products.

## 2 METHODOLOGY AND COMPUTATIONAL DETAILS

### 2.1 Molecular Dynamics (MD)

MD is a powerful computational method for modeling matter at the atomic scale. It consists in numerically solving Newton's equations of motion (equation 1) of particles (atoms or molecules) forming a system whose interactions are determined by an interatomic potential describing the forces between these particles.[31], [32]

$$\vec{F}_i = m_i \frac{d^2\vec{r}_i}{dt^2} = -\frac{\partial U}{\partial r_i}(\vec{r}_1, \vec{r}_2, \vec{r}_3, \dots, \vec{r}_N) \quad (1)$$

Solving Equation (1) requires the availability of the interatomic potential U, which must be a function of the coordinates of each atom i. It also requires two sets of initial conditions, positions and velocities, which can be derived from experiments or kinetic models.

Our study is based on the interaction of hydrocarbon species with electrodes described by a stainless steel surface composed of iron (Fe), chromium (Cr), molybdenum (Mo) and nickel (Ni). The potential describing the different interactions of our system can be written like this:

$$U_{system} = U_{HC} + U_{surf} + U_{HC-surf} \quad (2)$$

where $U_{HC}$ stands for the C-C, C-H and H-H interactions, $U_{surf}$ for the interactions between the surface atoms (Fe, Cr, Mo and Ni) and $U_{HC\text{-}surf}$ for the interactions between the atoms of the hydrocarbon molecules and those of the surface.

Reactive interatomic potentials including bond-breaking and bond-forming processes are necessary to describe $U_{HC}$. [33] The simplest and most robust potential is the REBO (Reactive Empirical Bond Order) potential, [34] which has been extended to AIREBO (Adaptive

Intermolecular Reactive Empirical Bond Order) to include long-range and torsional forces. [35], [36] Another class of reactive interatomic potentials includes partial charge dynamics in addition to bond order. Among them, COMB (Charge Optimized Many Body) and ReaxFF (Reactive Force Field) are the most commonly used. [37]–[39] Zarshenas et al. [40] performed ab-initio calculations using density functional theory (DFT) to select the best potential describing the reactions leading to the growth of hydrocarbon polymers on a silver substrate. Their DFT study predicted a reaction without an energy barrier, which is verified for REBO and the Aryanpour parameterization of ReaxFF,[41] whereas the other potentials indicated the existence of an unphysical reaction barrier.[40] Therefore, based on this work and considering the widespread use of the REBO potential for modeling interactions involving hydrocarbons [21], [40], [42]–[45] and its computational speed compared to ReaxFF,[46] the REBO potential was chosen in this work to describe $U_{HC}$. The REBO potential captures essential aspects of chemical bonding, especially for reactions in which covalent bonds are broken and formed. It distinguishes between radical and non-radical hydrocarbon species based on the concept of bond order. Radicals are modeled by assigning fractional bond orders to specific bonds. In contrast, non-radical hydrocarbon species are generally assigned integer bond orders corresponding to standard single, double or triple bonds, depending on their connectivity and the number of valence electrons.[34]

The interactions between the atoms of the surface ($U_{surf}$) are built using the embedded-atom method,[47]–[50] and the interactions between the atoms of the hydrocarbon molecules and the surface ($U_{HC\text{-}surf}$) were modeled using the Lennard-Jones (LJ) potential.[42], [51].

### 2.2 Input data

Input data, i.e. initial main neutral species, are obtained from a 1D fluid model[28], [29] that mimics the experimental conditions of a low pressure capacitively coupled Ar/$CH_4$ radio frequency plasma generated in a 2.54 cm discharge gap between 20 cm diameter electrodes. The operating conditions of the 1 D fluid model are listed in Table 1, and the corresponding initial neutral species are listed in Table 2.

**Table1:** Reference data of the 1 D fluid model from which the input data of our study are derived

| **Reference conditions** | |
|---|---|
| Temperature | 300 K |
| Pressure | 70 Pa |

| | |
|---|---|
| Vrf | 100 V |
| Frequency | 13.56 MHz |
| inter-electrode distance | 2.54 cm |
| Secondary emission electron probabilities | 0.01 |
| Percentage of argon | 96 |
| Percentage of methane | 4 |

**Table 2:** Main neutral species resulting from the 1 D fluid model used as input for the MD simulations. Argon is not included in our simulations [30].

| **Main neutral species** | **Molar fractions** |
|---|---|
| $H_2$ | $3.20 \times 10^{-2}$ |
| $CH_4$ | $1.40 \times 10^{-2}$ |
| $C_2H_4$ | $5.40 \times 10^{-3}$ |
| $C_2H$ | $3.20 \times 10^{-3}$ |
| $C_2H_2$ | $2.70 \times 10^{-3}$ |
| $CH_3$ | $2.30 \times 10^{-3}$ |

### 2.3 Simulation approach

Our approach to model the interaction processes between the neutral species, listed in Table 2, and the surface consists in depositing the species from a region above the surface and giving them initial velocities directed toward that surface, as shown in Figure 1 (a). The surface is a stainless steel slab that mimics the electrodes of an experimental device. Its composition is $Fe_{67}Cr_{17}Ni_{14}Mo_2$, i.e., 67% Fe, 17% Cr, 14% Ni, and 2% Mo. Periodic boundary conditions apply to the lateral boundaries (x-y) of the system (Figure 1 (a)) and deposition occurs in the z-direction (i.e., (001) orientation of the slab). The stainless steel slab of size $4.018 \times 4.018 \times 1.4$ $nm^3$ contains 1960 atoms and is divided into three zones as shown in Figure 1 (a). [40], [42], [52], [53] The bottom fixed atom zone prevents the move of the slab upon impact of species on the surface. The thermostated atoms zone (or stochastic zone) is the zone where a Langevin thermostat was applied to dissipate heat and absorb the energy of the upper zone. The freely moving atoms zone (or reaction zone) is the zone where the incident species and surface atoms can interact freely and without constraint. To mimic the flow of the species to the surface, the molecules are sent to the surface one after each other.

### 2.3.1 MD model for the calculation of the individual sticking probability

First simulations were performed to determine the individual sticking probability of the different species on a pristine surface [Figure 1 (a)] and on a surface covered with a previously deposited hydrocarbon film [Figure 1 (b)]. This C:H film contains a total of 975 carbon and hydrogen atoms with an H:C ratio of 0.6. The surface and the impinging species are set at room temperature (i.e., 300 K). Several simulations were performed. Each of them consists of the impingement of a molecule, 100 times, at a rate of one molecule every 2000 time steps (0.25 fs) over a 50 ps time. To obtain significant statistics, five simulations (with different initial positions and velocities) are performed for the deposition on both surfaces.

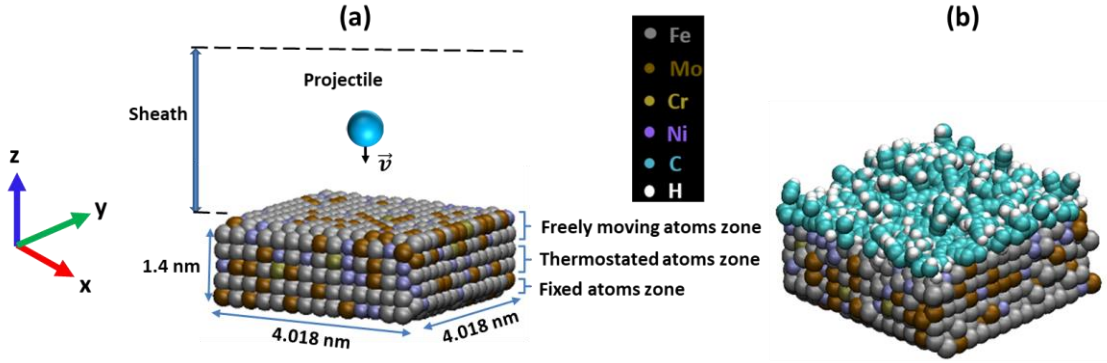


***Figure 1:*** *(a) Stainless steel slab mimicking pristine electrodes. It is composed of 67% Fe (silver color), 17% Cr (ochre color), 14% Ni (ice blue color), and 2% Mo (tan color). This surface is characterized by three zones (fixed, thermostated and reactive). (b) Same surface covered with a hydrocarbon film.*

### 2.3.2 MD model for the calculation of surface loss probabilities during C:H film growth.

The goal of these simulations is to determine the surface loss probabilities of each neutral species during the growth of the C:H film on the surface. To perform these simulations, all neutral species (49600 molecules in total) are sent to the pristine surface (Figure 1 (a)) at a rate of one molecule every 2000 time steps (i.e., every 500 fs) for a total time of 26 ns, taking into account the mole fraction of each species (Figure 2, 800 times repeating the cell framed in pink).

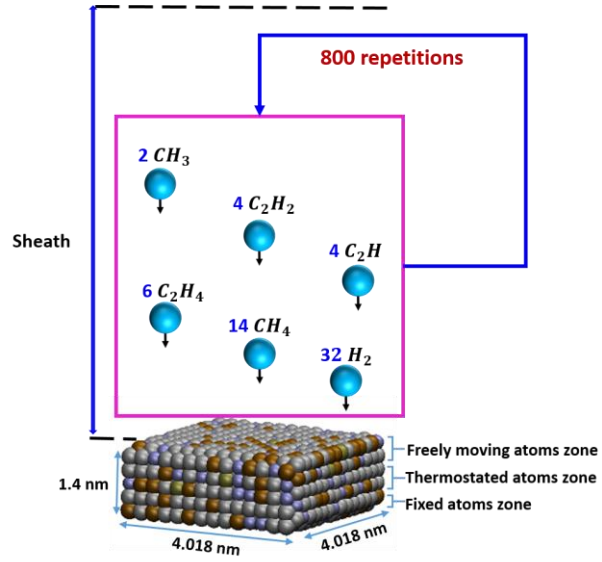


***Figure 2:*** *schematic representation of the initial layout of the system for sending all species together (one by one). The cell framed in pink represents the deposition of a cycle of neutral species repeated 800 times.*

Such a rate of deposition is high as often in MD simulation. The effect of this unphysically high flux is compensated by the substrate thermostat, which prevents unphysically high temperature increase due to energy transfer at impact.

The species are sequentially released, from a random position above the substrate, toward the surface with velocities randomly selected in a Maxwell-Boltzmann velocity distribution at 300 K. [54] [55]. Five simulation runs (with different initial velocity sets) were also performed.

All the MD simulations were carried out using the open-source code LAMMPS (Large-scale Atomic/Molecular Massively Parallel Simulator).[56] VMD software was used to visualize the MD results and Python scripts were written for data processing.[57], [58]

All plots in this study were obtained from the average over the five simulations with very small standard deviations (on the order of $10^{-4}$).

## 3 RESULTS AND DISCUSSION

### 3.1 Sticking probability (S) on pristine and hydrocarbon film covered surface.

In this section, we present the individual interaction of each species (i.e., the impingement of only 100 molecules of each neutral species per simulation, according to the procedure described in subsection 2.3.1) with a pristine surface (figure 1 (a)) and a surface covered with a C:H hydrocarbon film (figure 1 (b)) by determining the sticking probability (S). This describes the ratio between the number of atoms (or molecules) that adsorb or "stick" to the surface and the

total number of atoms that strike this surface during the same period. [21] Its value lies between 0 (no atom sticks) and 1 (all atoms that hit the surface stick) and is defined as follows:

$$S = \frac{N_{st}\ (with\ z \leq z_c)}{N} \tag{3}$$

where $N_{st}$ is the number of atoms or molecules sticking to the surface and N the total number of incident species, $z_c$ is the critical height, above which there are no more bonded atoms/molecules to the growing film. All species with $z > z_c$ are considered as reflected. The sticking probabilities of the different neutral species on a pristine stainless steel surface ($S_0$) and on a stainless steel surface covered with a C:H film ($S_c$) are presented in figure 3.

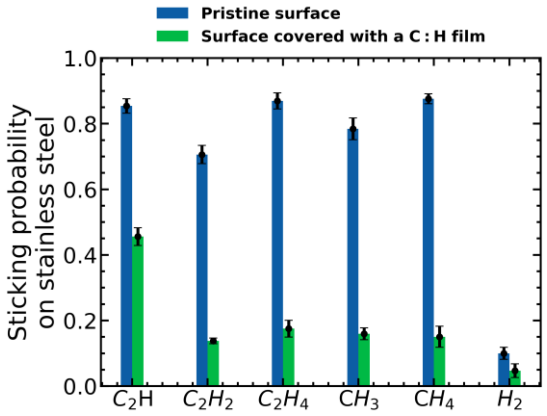


***Figure 3:*** *Sticking probability of the main neutral species of an argon-methane plasma on a pristine stainless steel surface (blue bars) and on a stainless steel surface covered with a C:H film previously deposited (green bars).*

It can be observed that $S_0$ of all neutral species on a pristine surface (figure 3 blue bar) is high (around 0.8, except for $H_2$) compared to the values $S_c$ on the surface covered with the C:H film (figure 3 green bars). This is due to the fact that on the pristine surface the species easily find a stable anchoring site to be able to stick whereas on the surface covered with the C:H film, the search for a reactive site is more difficult. With the exception of the $C_2H$ radical (which has the highest $S_c$ because of its very reactive character), the other species have $S_c$ lower than 0.2. For the $CH_3$ radical, the low $S_c$ is explained by the fact that this molecule requires dangling bond sites on the surface of the C:H film to be able to stick. [22], [59]–[61]

The sticking probability of $C_2H$ obtained in our study is rather different from the one used in the literature (about 0.8) [15], [16], and supposed to be obtained on amorphous C:H film surfaces. The value obtained in our study, which is close to that in the literature, is the value calculated on a pristine surface, whereas the value calculated on a C:H film is ½ times lower than the value used in the literature while it was expected to be similar. Before drawing any conclusion on this discrepancy, in the next section we will discuss the surface reaction

probabilities of each neutral species when releasing all the initial neutral species one after each other as shown in Fig. 2.

**3.2 Surface loss probabilities of main neutrals species during film growth.**

Various phenomena can occur during the interaction of neutral species with the surface. They can return to the gas phase with a reflection probability r, react with other species at the surface to form volatile hydrocarbons ($C_xH_y$) with a recombination probability γ (these volatile species diffuse at the surface and are then desorbed into the gas phase), or form a chemical bond with the surface with a sticking probability S (film formation). These last two events result in the loss of the particle from the gas phase and are described by the surface loss (or surface reaction) probability β =S+γ. [13], [15], [62] The set of these events for a single specie is shown in Figure 4 and is summarized by the following expression:

$$r + S + \gamma = r + \beta = 1 \tag{4}$$

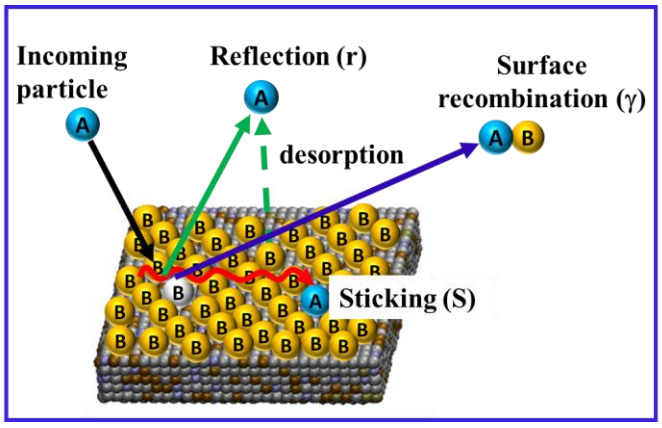


***Figure 4:*** *Illustration of the surface mechanisms (reflection, recombination and sticking) during the interaction of a neutral species with the surface. (adapted from [13])*

Figures 5 (a)-(c) represent, respectively, the temporal evolutions of the sticking probability S, the surface recombination probability γ and the surface loss probability β of each neutral species during the growth of the C:H surface film from a pristine surface. For this part, the neutral species were sent together one after each other, as described in subsection 2.3.2, to achieve a collective behavior that would allow the experiments to be mimicked.

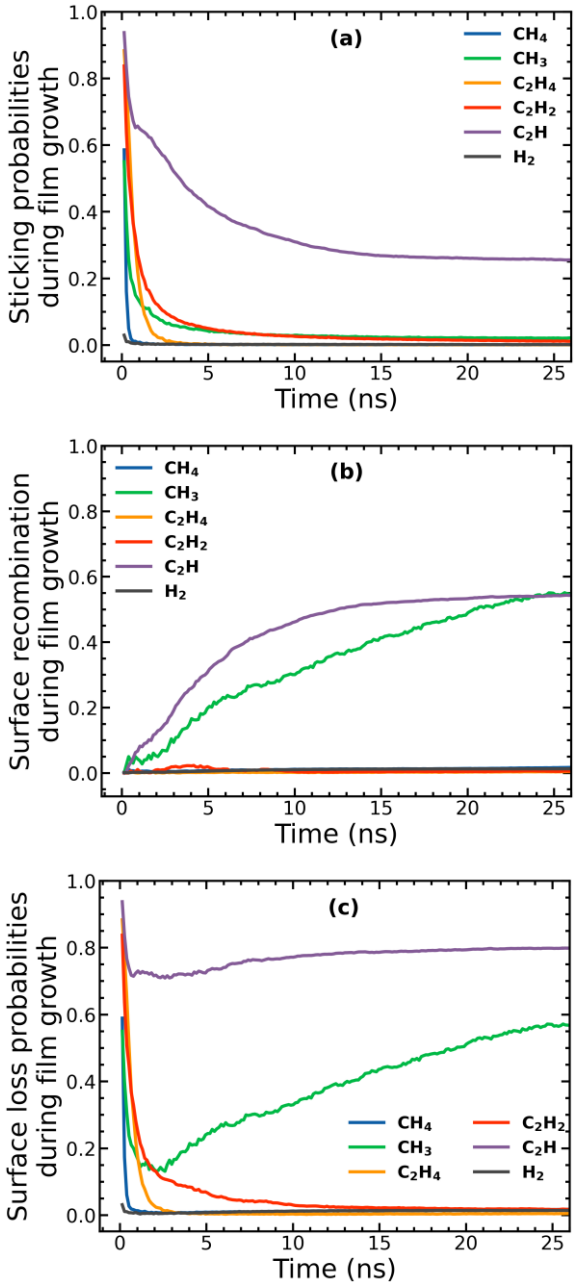


***Figure 5:*** *Temporal evolutions of the sticking probability S (a), surface recombination probabilities $\gamma$ (b) and surface loss probabilities $\beta$ (c) of each neutral species during the growth of the C:H film.*

In Figure 5 (a) we see that, at the early time, (between 0 and 1 ns), except for $H_2$, the sticking probabilities of the stable hydrocarbon species, namely $CH_4$, $C_2H_2$, $C_2H_4$, are high (between 0.6 and 0.9), and then decrease as the C:H film grows on the surface, becoming almost 0 after 5 ns. This behavior is due to the fact that these molecules stick easily when the surface is pristine (i.e., without a C:H film on the surface), but when the C:H film starts to form onto the surface, their sticking is lowered, as also shown in Figure 3 for the individual sticking probabilities. It is also observed that these stable molecules do not participate in the surface reactions to form

volatile species, since their surface recombination probabilities are almost zero over time [Figure 5 (b)]. This is justified by the fact that these species are very little reactive and thus less involved in the formation of new species, [13], [20] . This leads finally to low surface loss probabilities for all these stable species (Figure 5 (c)) and indicates that they return to the gas phase after the very first nanoseconds without any change.

In the literature, the growth of C:H films in hydrocarbon plasmas is assumed to be due to radicals and the stable species are usually considered to be fully reflected by the surface. [13], [18], [20], [28] This assumption is true when the surface is no longer pristine (presence of a C:H film). At the beginning of the deposition, we observe that the stable species are not fully reflected when the surface is pristine, and they contribute to the growth. They are fully reflected only once the C:H first layers are formed, screening thus the interactions with the stainless steel surface. So their role in the formation of the first monolayer should not be neglected.

However, in experiments, it is very unlikely that electrodes are pristine at the ignition of a plasma, which means that the behavior of the stable species in the first times observed in our simulations is not experimentally accessible. On the other hand, their behavior in the presence of a C:H film on the surface is consistent with the literature [13], [15], [16], [20], [63]. Furthermore, Sharma et al.[24] also observed through molecular dynamics simulations that these species ($H_2$, $CH_4$, $C_2H_2$, $C_2H_4$, and $H_2$) were fully reflected after their interaction with an C:H surface at room temperature. Nevertheless, the interaction of incident neutral species with a pristine surface is relevant because it provides information about the contribution of stable species to the formation of the first hydrocarbon monolayer in the very first times of simulation or plasma ignition, after that the role of the substrate is quickly screened by the growing film.

For the $CH_3$ radical [Fig. 5 (a)], S is high in the first instants (between 0 and 1 ns) and becomes constant to a very low value (0.02) after 5 ns, which implies that this radical contributes to the film growth only at the very beginning. Indeed, once a C:H film is formed on the surface, the $CH_3$ radical needs available dangling bond sites to be able to stick[22], [59], which is much more difficult.

In a review paper by Jacob [20] about the surface growth of hydrocarbon films, the sticking probability of $CH_3$ is shown to be negligible. This probability can increase depending on the available surface dangling bonds, [64], [65] which are created by ionic or atomic hydrogen bombardment.[66], [67] Atomic hydrogen and ions are not considered in the present study and this effect cannot be evidenced by our simulations.

Moreover, the presence of species more reactive than $CH_3$, such as $C_2H$, can reduce its sticking to the surface. This was observed, for example, in the work of Bauer et al [59] studying film

deposition in pulsed inductively coupled methane plasmas, where the authors found that the $CH_3$ radical played a role in film growth only at pressures where highly reactive radicals such as $C_2H$ were deactivated.

We can also observe in Figure 5 (b) that the surface recombination probability $\gamma(CH_3)$ increases nearly linearly with time showing that $CH_3$ does contribute to the formation of volatile products, and thus can play a role in the gas-phase plasma chemistry. These results lead to a high $\beta(CH_3)$ in the early time deposition (< 1 ns), which then decreases to a minimum value and then slowly increases [due to the behavior of $\gamma(CH_3)$] reaching a value around 0.6 after 22 ns. In the literature [15], [16], [68], $\beta(CH_3)$ is considered to be smaller than 0.01, since the surface loss probability is very often expressed in terms of the sticking coefficient,[18] and thus $\gamma(CH_3)$ is largely neglected. The present results show that $\gamma(CH_3)$ cannot be neglected and should therefore be taken into account.

Concerning the $C_2H$ radical, it is observed that $S(C_2H)$ [Figure 5 (a)] is the highest in the first instants (<1 ns) and then slowly decreases but remains larger than the sticking probabilities of the other molecules. For example, we can see that $\beta(C_2H)$ is higher than $\beta(CH_3)$, which is consistent with the work of Sharma et al. [24], who finds that radicals with fewer hydrogen atoms have a higher surface loss probabilities than those with more hydrogen atoms. These observations indicate that the $C_2H$ radical is the main precursor of the growth of the C:H film on the electrode surface. This radical is one of the species that do not require a specific adsorption site on the surface to chemisorbs due to its highly reactive nature.[13], [17], [18], [59] However, we can observe that the decrease of $S(C_2H)$ [Figure 5 (a)] is counterbalanced by the temporal increase of $\gamma$ ($C_2H$), leading to an almost constant $\beta$ ($C_2H$) [Figure 5 (c)] (around a value of 0.8) after 1 ns.

This value of 0.8 for $\beta(C_2H)$ agrees well with the experimental value obtained by Hopf et al. on amorphous hydrogenated carbon film surfaces [15]. These authors obtained a value of $\beta$ ($C_2H$) =0.9 for acetylene-based discharges and $\beta$ ($C_2H$) =0.8 for other hydrocarbon discharges. However, the authors assumed that $\gamma$ ($C_2H$) is lower than 0.1 and thus that $S(C_2H) \approx 0.8$ for all hydrocarbon discharges. This value of $S(C_2H)$ is commonly used in the literature [69], particularly for kinetic models of hydrocarbon plasmas. [14], [18], [28], [29], [70]–[72] These values are not in agreement with those obtained in our simulations $S(C_2H)$=0.25 and $\gamma$ ($C_2H$)=0.55 at steady-state after 15 ns. This significant difference might be due to the fact that the authors consider only the formation of nonreactive volatile products when estimating the recombination probability $\gamma$ and therefore assume that the $C_2H$ radical forms only $C_2H_2$ in the

abstraction reaction: $C_2H$ + H (surface) → $C_2H_2$ + surface. The authors consider that the surface recombination probability corresponding to this reaction is lower than 0.1. In contrast, our study includes both volatile reactive and non-reactive product formation at the surface. The present MD simulations indicate that the formation of reactive volatile products at the surface is important and cannot be neglected, as it will be shown also in section 3.4.

In addition, the authors [15] determined the surface loss probabilities of radicals at the surface of C:H films with a hydrogen to carbon ratio greater than or equal to 1, while in our study this ratio is smaller than 1 for the film grown by MD. This difference in the H/C ratio can play a role as shown in [25].

This could justify the underestimation of γ ($C_2H$) in their study because C:H films with an H:C ratio ≥ 1 are softer and therefore lead to deeper penetration of atoms into the hydrocarbon film, increasing the sticking probability. [24]–[26] Moreover, it is known that the surface loss probability of radicals strongly depends on plasma parameters such as temperature or surface composition.[26]

All the values obtained at the end of the simulation are summarized in Table 3 for each species.

***Table 3:*** *Values of sticking probability (S), surface recombination probability (γ) and surface loss probability (β) of each species after C:H film growth, values available in the literature are put in brackets.*

| **Species** | **S** | **γ** | **β** |
|---|---|---|---|
| **$C_2H$** | 0.25 (*0.8* [15]) | 0.55 (*<0.1* [15]) | 0.8 (*0.8/0.9* [15]) |
| **$CH_3$** | 0.02 (*~$10^{-4}$* [66]) | 0.54 | 0.56 (*<0.01* [15]) |
| **$CH_4$** | <0.001 | 0.02 | 0.02 |
| **$C_2H_4$** | 0.001 | 0.004 | 0.005 |
| **$C_2H_2$** | 0.014 | 0.006 | 0.02 |
| **$H_2$** | 0.002 | 0.008 | 0.01 |

Differences are observed between the values of the sticking probabilities of the different neutral species obtained in Figure 3 for the covered surface and those obtained at the end of the film growth (Table 3). A first reason is that the simulations carried out to obtain the values of Figure 3 are carried out over a period of 50 ps and species are sent individually, whereas in those of Table 3 the species are sent all together over a time of 26 ns. In the latter case, this may lead to competition between species for finding a place to stick leading to a decrease of the sticking

coefficient. Also, as can be seen in figure 5, at a certain point in the simulation, there is a saturation of the sticking probability of the individual species. This means that the values obtained after the growth of the film (Table 3) are expected to be closer to the real conditions than the values in Figure 3.

### 3.4 Gas phase species during growth of C:H films.

Figure 6 shows the time evolution of the $C_n$ carbon clusters (i.e., all molecules with n carbon atoms, regardless of the number of hydrogen atoms), here limited to $C_1$ to $C_{>9}$, formed by surface reactions during the growth of the C:H film. It should be noted that for the $C_1$ and $C_2$ clusters, the initial reflected molecules and the produced molecules corresponding to an initial species, are not counted. Cluster $C_{>9}$ represents the sum of all clusters with size greater than 9. Large clusters are formed through direct interaction of impinging species with the surface or by rapid reactions between molecules reemitted in the gas phase just above the surface. It can be observed that, with the exception of the $C_1$ cluster quantity, which is almost zero, the other $C_2$-$C_{>9}$ clusters show an approximately linear temporal evolution with $C_3$ and $C_4$ clusters being the two main clusters over time. These observations are consistent with the evolutions of the surface recombination probabilities $\gamma(CH_3)$ and $\gamma(C_2H)$ in Figure 5 (b) as these impinging molecules are at the origin of the reemitted $C_3$ and $C_4$ clusters.

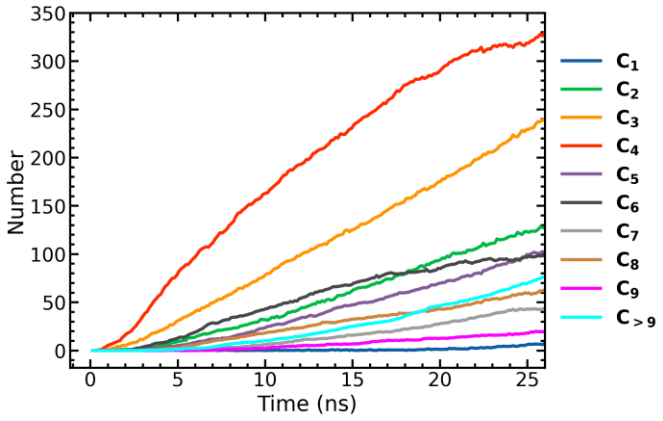


***Figure 6:*** *Temporal evolution of the $C_1$ to $C_{>9}$ clusters re-emitted during the growth of the C:H film in the gas phase. The molecules corresponding to the initial species are not included in the count of $C_1$ and $C_2$ clusters. The $C_{>9}$ clusters represent the sum of all clusters whose size is larger than 9 carbon atoms.*

Figure 7 shows the mass spectrum of the species re-emitted in the gas phase, at the end of the runs (26 ns). The initially stable non-reactive hydrocarbon species ($CH_4$, $C_2H_2$, and $C_2H_4$) are

the species, most re-emitted in the gas phase. This is consistent with the fact that they are nearly totally reflected after surface interactions.

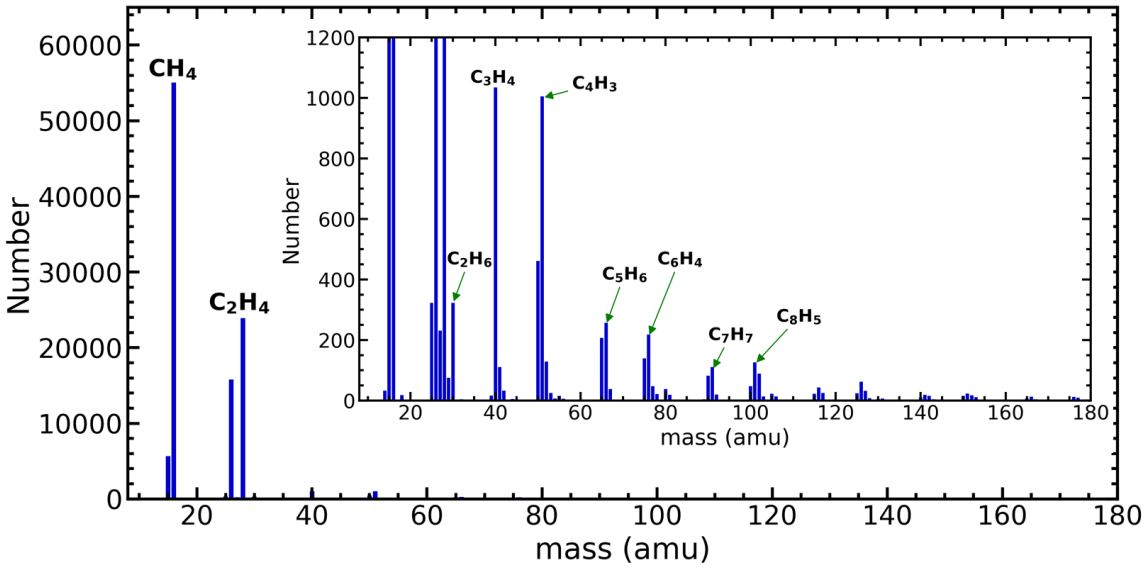


***Figure 7:*** *Mass spectra of the final species re-emitted after growth of the C:H film. The inner figure represents a zoom to highlight the species in small quantity (especially the emitted species that are different from the incident species).*

In the inset of figure 7, we have identified some of the main other volatile species formed at the surface. We can observe the presence of reactive (e.g., $C_4H_2$, $C_4H_3$, $C_6H_3$, etc.) and non-reactive [e.g., $C_2H_6$, $C_3H_4$ ($CH{\equiv}C{-}CH_3$), etc.] species. These observations highlight that the reactions of radicals on the surface lead not only to the formation of non-reactive volatile products, as shown in the literature [13], [15], but also to reactive volatile products[13], [15][13], [15][13], [15]. This confirms that the formation of reactive species has to be considered when calculating the probability of surface recombination. Moreover, species such as $C_4H_2$, $C_4H_3$, and $C_6H_3$ are widely known in hydrocarbon plasmas for contributing to the growth of films and large molecules. [13], [17], [18], [73] In a previous work [30], their importance, as well as the one of $C_6H_4$, was reported for the growth of large molecules in volume phase. This means that the amount of reactive and non-reactive volatile products is significant and therefore cannot be neglected. In addition, the volatile reactive species that are re-emitted in the gas phase may contribute to the reaction mechanisms that lead to the growth of hydrocarbon chains or solid particles in the volume phase. In the previous section, we noted that the surface recombination probability resulting in a reactive or non-reactive volatile molecule is not negligible, especially for $CH_3$ and $C_2H$ radicals. Although this quantity is difficult to measure experimentally,[15] its rough estimation (by, for example, neglecting the formation of reactive volatile products or

underestimating the amount of non-reactive volatile products) leads to a large loss of information in the interpretation of the surface loss probabilities of the $CH_3$ and $C_2H$ radicals. The separate calculation of the sticking and surface recombination probabilities is therefore necessary to obtain a clear overview and understanding of the behavior of the different radical species during their interaction with the surface. As shown by the present study, the separate calculation of these two quantities is more accessible through molecular dynamics simulations.

## 4 CONCLUSION

In this study, reactive molecular dynamics was used to investigate the surface loss probabilities of various neutral species ($H_2$, $CH_4$, $C_2H_4$, $C_2H$, $C_2H_2$, and $CH_3$) in an argon-methane plasma. The sticking probabilities of each of these species were calculated on both a pristine surface and a surface coated with a C:H film. The results showed that the sticking probabilities were higher on a pristine surface than on the surface covered with the C:H film. In the subsequent simulations, the neutral species were sent to a pristine surface together and their sticking probability (S) and surface recombination probability ($\gamma$) were determined. Both reactive and non-reactive volatiles were considered in the $\gamma$ estimation, in contrast to the literature which only considers non-reactive volatiles. This analysis provided valuable information on the surface loss probability ($\beta = S + \gamma$) of the main neutral species in the $Ar/CH_4$ plasma during C:H film growth. The study revealed that stable species, particularly $CH_4$, $C_2H_4$, and $C_2H_2$, contributed to the initial formation of the hydrocarbon films and that they were subsequently fully reflected with probabilities S and $\gamma$ very close to zero. Among the radicals, it was observed that $CH_3$ contributed more to the formation of volatile species than to the growth of the C:H film, while the $C_2H$ radical was identified as the main precursor of film growth and volatile species formation with a surface loss probability (0.8) that corresponds to the typical value found in the literature. However, a difference was observed between the values of $S(C_2H)$ and $\gamma(C_2H)$ and those estimated in the literature. $C_3H_4$ and $C_4H_3$ species were identified as the main molecules (reactive and non-reactive) re-emitted during the growth of the C:H film. Although this study highlights the importance of recombination processes at the surface, which are generally underestimated in existing kinetic models, this work may have certain limitations due to the H/C ratio of the resulting film and the fact that the effects of charged species impinging on the surface are not considered. It paves the way for future simulations involving ions in the deposition processes, keeping in mind that the corresponding flux remains small compared to neutral fluxes.

## ACKNOWLEDGMENTS

This work has been supported by the National Scholarship Agency of Gabon (ANBG) and the French National Research Agency (ANR) through the MONA project (ANR-18-CE30-0016). We are grateful to the Fédération Calcul Scientifique et Modélisation Orléans Tours (CaSciModOT) for the numerical resources made available to us.

## CONFLICT OF INTEREST

The authors declare no conflict of interest

## DATA AVAILABILITY STATEMENT

Data are available from the authors upon reasonable request.

## REFERENCES

[1] M. Jiménez-Redondo, I. Tanarro, and V. J. Herrero, "Time evolution of neutral and charged species in Ar/$C_2H_2$ capacitively-coupled RF discharges," *Plasma Sources Sci. Technol.*, vol. 31, no. 6, p. 065003, Jun. 2022, doi: 10.1088/1361-6595/ac70f8.

[2] S. Stoykov, C. Eggs, and U. Kortshagen, "Plasma chemistry and growth of nanosized particles in a $C_2H_2$ RF discharge," *J. Phys. D: Appl. Phys.*, vol. 34, no. 14, pp. 2160–2173, Jul. 2001, doi: 10.1088/0022-3727/34/14/312.

[3] I. B. Denysenko, E. Wahl, S. Labidi, M. Mikikian, H. Kersten, and T. Gibert, "Effects of process conditions on the chemistry of an Ar/$C_2H_2$ dust-forming plasma," *Plasma Process Polym*, vol. 16, no. 6, p. 1800209, Jun. 2019, doi: 10.1002/ppap.201800209.

[4] M. Tanemura *et al.*, "Growth of aligned carbon nanotubes by plasma-enhanced chemical vapor deposition: Optimization of growth parameters," *Journal of Applied Physics*, vol. 90, no. 3, pp. 1529–1533, Aug. 2001, doi: 10.1063/1.1382848.

[5] K. Ostrikov, "*Colloquium* : **Reactive plasmas as a versatile nanofabrication tool**," *Rev. Mod. Phys.*, vol. 77, no. 2, pp. 489–511, Jun. 2005, doi: 10.1103/RevModPhys.77.489.

[6] *Carbon Nanomaterials and their Nanocomposite-Based Chemiresistive Gas Sensors*. Elsevier, 2023. doi: 10.1016/C2019-0-04471-8.

[7] A. M. Díez-Pascual, Ed., *Carbon-Based Nanomaterials 2.0*. MDPI, 2023. doi: 10.3390/books978-3-0365-6548-4.

[8] M. Frenklach and H. Wang, "Detailed surface and gas-phase chemical kinetics of diamond deposition," *Phys. Rev. B*, vol. 43, no. 2, pp. 1520–1545, Jan. 1991, doi: 10.1103/PhysRevB.43.1520.

[9] K. Kobayashi, N. Mutsukura, and Y. Machi, “Surface properties of diamond and diamond-like hydrogenated amorphous carbon films resulting from r.f. plasma etching,” *Thin Solid Films*, vol. 200, no. 1, pp. 139–145, May 1991, doi: 10.1016/0040-6090(91)90036-W.

[10] A. H. Lettington, “Applications of diamond-like carbon thin films,” *Carbon*, vol. 36, no. 5–6, pp. 555–560, 1998, doi: 10.1016/S0008-6223(98)00062-1.

[11] A. A. Khan, J. A. Woollam, and Y. Chung, “High frequency capacitance-voltage and conductance-voltage characteristics of d.c. sputter deposited a-carbon/silicon MIS structures,” *Solid-State Electronics*, vol. 27, no. 4, pp. 385–391, Apr. 1984, doi: 10.1016/0038-1101(84)90173-4.

[12] L. Hu, D. S. Hecht, and G. Grüner, “Carbon Nanotube Thin Films: Fabrication, Properties, and Applications,” *Chem. Rev.*, vol. 110, no. 10, pp. 5790–5844, Oct. 2010, doi: 10.1021/cr9002962.

[13] J. Benedikt, “Plasma-chemical reactions: low pressure acetylene plasmas,” *J. Phys. D: Appl. Phys.*, vol. 43, no. 4, p. 043001, Feb. 2010, doi: 10.1088/0022-3727/43/4/043001.

[14] I. B. Denysenko *et al.*, “Plasma properties as function of time in Ar/$C_2H_2$ dust-forming plasma,” *J. Phys. D: Appl. Phys.*, vol. 53, no. 13, p. 135203, Mar. 2020, doi: 10.1088/1361-6463/ab6625.

[15] C. Hopf, K. Letourneur, W. Jacob, T. Schwarz-Selinger, and A. von Keudell, “Surface loss probabilities of the dominant neutral precursors for film growth in methane and acetylene discharges,” *Appl. Phys. Lett.*, vol. 74, no. 25, pp. 3800–3802, Jun. 1999, doi: 10.1063/1.124184.

[16] A. von Keudell, C. Hopf, T. Schwarz-Selinger, and W. Jacob, “Surface loss probabilities of hydrocarbon radicals on amorphous hydrogenated carbon film surfaces: Consequences for the formation of re-deposited layers in fusion experiments,” *Nucl. Fusion*, vol. 39, no. 10, pp. 1451–1462, Oct. 1999, doi: 10.1088/0029-5515/39/10/307.

[17] J. R. Doyle, “Chemical kinetics in low pressure acetylene radio frequency glow discharges,” *Journal of Applied Physics*, vol. 82, no. 10, pp. 4763–4771, Nov. 1997, doi: 10.1063/1.366333.

[18] K. De Bleecker, A. Bogaerts, and W. Goedheer, “Detailed modeling of hydrocarbon nanoparticle nucleation in acetylene discharges,” *Phys. Rev. E*, vol. 73, no. 2, p. 026405, Feb. 2006, doi: 10.1103/PhysRevE.73.026405.

[19] W. Eckstein, *Computer Simulation of Ion-Solid Interactions*, vol. 10. in Springer Series in Materials Science, vol. 10. Berlin, Heidelberg: Springer Berlin Heidelberg, 1991. doi: 10.1007/978-3-642-73513-4.

[20] W. Jacob, “Surface reactions during growth and erosion of hydrocarbon films,” *Thin Solid Films*, vol. 326, no. 1–2, pp. 1–42, Aug. 1998, doi: 10.1016/S0040-6090(98)00497-0.

[21] L. Schwaederlé, P. Brault, C. Rond, and A. Gicquel, “Molecular Dynamics Calculations of CH3 Sticking Coefficient onto Diamond Surfaces,” *Plasma Processes and Polymers*, vol. 12, no. 8, pp. 764–770, 2015, doi: 10.1002/ppap.201400223.

[22] E. D. de Rooij, A. W. Kleyn, and W. J. Goedheer, “Sticking of hydrocarbon radicals on different amorphous hydrogenated carbon surfaces: a molecular dynamics study,” *Phys. Chem. Chem. Phys.*, vol. 12, no. 42, p. 14067, 2010, doi: 10.1039/c0cp00637h.

[23] K. Ohya *et al.*, “Simulation of hydrocarbon reflection from carbon and tungsten surfaces and its impact on codeposition patterns on plasma facing components,” *Journal of Nuclear Materials*, vol. 390–391, pp. 72–75, Jun. 2009, doi: 10.1016/j.jnucmat.2009.01.072.

[24] A. R. Sharma, R. Schneider, U. Toussaint, and K. Nordlund, “Hydrocarbon radicals interaction with amorphous carbon surfaces,” *Journal of Nuclear Materials*, vol. 363–365, pp. 1283–1288, Jun. 2007, doi: 10.1016/j.jnucmat.2007.01.180.

[25] D. A. Alman and D. N. Ruzic, “Molecular dynamics calculation of carbon/hydrocarbon reflection coefficients on a hydrogenated graphite surface,” *Journal of Nuclear Materials*, vol. 313–316, pp. 182–186, Mar. 2003, doi: 10.1016/S0022-3115(02)01428-9.

[26] D. A. Alman and D. N. Ruzic, “Molecular Dynamics Simulation of Hydrocarbon Reflection and Dissociation Coefficients from Fusion-Relevant Carbon Surfaces,” *Physica Scripta*, vol. T111, no. 1, p. 145, 2004, doi: 10.1238/Physica.Topical.111a00145.

[27] P. Träskelin, E. Salonen, K. Nordlund, J. Keinonen, and C. H. Wu, “Molecular dynamics simulations of CH3 sticking on carbon surfaces, angular and energy dependence,” *Journal of Nuclear Materials*, vol. 334, no. 1, pp. 65–70, Aug. 2004, doi: 10.1016/j.jnucmat.2004.04.334.

[28] G. Tetard, A. Michau, S. Prasanna, J. Mougenot, P. Brault, and K. Hassouni, “Discharge dynamics, plasma kinetics and gas flow effect in argon–acetylene discharges,” *Plasma Sources Sci. Technol.*, vol. 30, no. 10, p. 105015, Oct. 2021, doi: 10.1088/1361-6595/ac2a17.

[29] G. Tetard, A. Michau, S. Prasanna, J. Mougenot, P. Brault, and K. Hassouni, “Molecular growth paths and dust-particles nucleation precursors in Ar/$C_2H_2$ low pressure discharges,” *Plasma Processes & Polymers*, vol. 19, no. 5, p. 2100204, May 2022, doi: 10.1002/ppap.202100204.

[30] G. O. Kandjani, P. Brault, M. Mikikian, G. Tetard, A. Michau, and K. Hassouni, “Molecular dynamics simulations of reactive neutral chemistry in an argon-methane plasma,” *Plasma Processes & Polymers*, vol. 20, no. 4, p. 2200192, Apr. 2023, doi: 10.1002/ppap.202200192.

[31] E. C. Neyts and P. Brault, “Molecular Dynamics Simulations for Plasma-Surface Interactions: Molecular Dynamics Simulations…,” *Plasma Process. Polym.*, vol. 14, no. 1–2, p. 1600145, Jan. 2017, doi: 10.1002/ppap.201600145.

[32] D. B. Graves and P. Brault, “Molecular dynamics for low temperature plasma–surface interaction studies,” *J. Phys. D: Appl. Phys.*, vol. 42, no. 19, p. 194011, Oct. 2009, doi: 10.1088/0022-3727/42/19/194011.

[33] T. Liang *et al.*, “Reactive Potentials for Advanced Atomistic Simulations,” *Annu. Rev. Mater. Res.*, vol. 43, no. 1, pp. 109–129, Jul. 2013, doi: 10.1146/annurev-matsci-071312-121610.

[34] D. W. Brenner, O. A. Shenderova, J. A. Harrison, S. J. Stuart, B. Ni, and S. B. Sinnott, “A second-generation reactive empirical bond order (REBO) potential energy expression for hydrocarbons,” *J. Phys.: Condens. Matter*, vol. 14, no. 4, pp. 783–802, Feb. 2002, doi: 10.1088/0953-8984/14/4/312.

[35] S. J. Stuart, A. B. Tutein, and J. A. Harrison, “A reactive potential for hydrocarbons with intermolecular interactions,” *The Journal of Chemical Physics*, vol. 112, no. 14, pp. 6472–6486, Apr. 2000, doi: 10.1063/1.481208.

[36] T. C. O’Connor, J. Andzelm, and M. O. Robbins, “AIREBO-M: A reactive model for hydrocarbons at extreme pressures,” *The Journal of Chemical Physics*, vol. 142, no. 2, p. 024903, Jan. 2015, doi: 10.1063/1.4905549.

[37] J. Yu, S. B. Sinnott, and S. R. Phillpot, “Charge optimized many-body potential for the Si / SiO 2 system,” *Phys. Rev. B*, vol. 75, no. 8, p. 085311, Feb. 2007, doi: 10.1103/PhysRevB.75.085311.

[38] T.-R. Shan, B. D. Devine, J. M. Hawkins, A. Asthagiri, S. R. Phillpot, and S. B. Sinnott, “Second-generation charge-optimized many-body potential for Si / SiO 2 and amorphous silica,” *Phys. Rev. B*, vol. 82, no. 23, p. 235302, Dec. 2010, doi: 10.1103/PhysRevB.82.235302.

[39] A. C. T. van Duin, S. Dasgupta, F. Lorant, and W. A. Goddard, “ReaxFF: A Reactive Force Field for Hydrocarbons,” *J. Phys. Chem. A*, vol. 105, no. 41, pp. 9396–9409, Oct. 2001, doi: 10.1021/jp004368u.

[40] M. Zarshenas, K. Moshkunov, B. Czerwinski, T. Leyssens, and A. Delcorte, “Molecular Dynamics Simulations of Hydrocarbon Film Growth from Acetylene Monomers and Radicals: Effect of Substrate Temperature,” *J. Phys. Chem. C*, vol. 122, no. 27, pp. 15252–15263, Jul. 2018, doi: 10.1021/acs.jpcc.8b01334.

[41] M. Aryanpour, A. C. T. van Duin, and J. D. Kubicki, “Development of a Reactive Force Field for Iron−Oxyhydroxide Systems,” *J. Phys. Chem. A*, vol. 114, no. 21, pp. 6298–6307, Jun. 2010, doi: 10.1021/jp101332k.

[42] P. Brault, M. Ji, D. Sciacqua, F. Poncin-Epaillard, J. Berndt, and E. Kovacevic, “Insight into acetylene plasma deposition using molecular dynamics simulations,” *Plasma Processes & Polymers*, vol. 19, no. 1, p. 2100103, Jan. 2022, doi: 10.1002/ppap.202100103.

[43] J. J. Végh and D. B. Graves, “Molecular Dynamics Simulations of $Ar^+$-Organic Polymer Interactions,” *Plasma Process. Polym.*, vol. 6, no. 5, pp. 320–334, May 2009, doi: 10.1002/ppap.200800223.

[44] E. Neyts, M. Eckert, and A. Bogaerts, “Molecular Dynamics Simulations of the Growth of Thin A-C:H Films Under Additional Ion Bombardment: Influence of the Growth Species and the Ar+ Ion Kinetic Energy,” *Chem. Vap. Deposition*, vol. 13, no. 6–7, pp. 312–318, Jul. 2007, doi: 10.1002/cvde.200606551.

[45] W. L. Quan *et al.*, “Molecular dynamics simulation of hydrogenated carbon film growth from CH radicals,” *Applied Surface Science*, vol. 263, pp. 339–344, Dec. 2012, doi: 10.1016/j.apsusc.2012.09.057.

[46] S. J. Plimpton and A. P. Thompson, “Computational aspects of many-body potentials,” *MRS Bull.*, vol. 37, no. 5, pp. 513–521, May 2012, doi: 10.1557/mrs.2012.96.

[47] M. S. Daw, S. M. Foiles, and M. I. Baskes, “The embedded-atom method: a review of theory and applications,” *Materials Science Reports*, vol. 9, no. 7–8, pp. 251–310, Mar. 1993, doi: 10.1016/0920-2307(93)90001-U.

[48] X. W. Zhou *et al.*, “Atomic scale structure of sputtered metal multilayers,” *Acta Materialia*, vol. 49, no. 19, pp. 4005–4015, Nov. 2001, doi: 10.1016/S1359-6454(01)00287-7.

[49] X. W. Zhou, R. A. Johnson, and H. N. G. Wadley, “Misfit-energy-increasing dislocations in vapor-deposited CoFe/NiFe multilayers,” *Phys. Rev. B*, vol. 69, no. 14, p. 144113, Apr. 2004, doi: 10.1103/PhysRevB.69.144113.

[50] C.-M. Lin and H.-L. Tsai, “Evolution of microstructure, hardness, and corrosion properties of high-entropy Al0.5CoCrFeNi alloy,” *Intermetallics*, vol. 19, no. 3, pp. 288–294, Mar. 2011, doi: 10.1016/j.intermet.2010.10.008.

[51] D. W. Jacobson and G. B. Thompson, “Revisting Lennard Jones, Morse, and N-M potentials for metals,” *Computational Materials Science*, vol. 205, p. 111206, Apr. 2022, doi: 10.1016/j.commatsci.2022.111206.

[52] D. Toton, C. D. Lorenz, N. Rompotis, N. Martsinovich, and L. Kantorovich, “Temperature control in molecular dynamic simulations of non-equilibrium processes,” *J.*

*Phys.: Condens. Matter*, vol. 22, no. 7, p. 074205, Feb. 2010, doi: 10.1088/0953-8984/22/7/074205.

[53] S. Wang and K. Komvopoulos, "Structure evolution during deposition and thermal annealing of amorphous carbon ultrathin films investigated by molecular dynamics simulations," *Sci Rep*, vol. 10, no. 1, p. 8089, Dec. 2020, doi: 10.1038/s41598-020-64625-w.

[54] G. E. P. Box and M. E. Muller, "A Note on the Generation of Random Normal Deviates," *Ann. Math. Statist.*, vol. 29, no. 2, pp. 610–611, Jun. 1958, doi: 10.1214/aoms/1177706645.

[55] S. Sharma, P. Kumar, and R. Chandra, "Introduction to Molecular Dynamics," in *Molecular Dynamics Simulation of Nanocomposites Using BIOVIA Materials Studio, Lammps and Gromacs*, Elsevier, 2019, pp. 1–38. doi: 10.1016/B978-0-12-816954-4.00001-2.

[56] A. P. Thompson *et al.*, "LAMMPS - a flexible simulation tool for particle-based materials modeling at the atomic, meso, and continuum scales," *Computer Physics Communications*, vol. 271, p. 108171, Feb. 2022, doi: 10.1016/j.cpc.2021.108171.

[57] W. Humphrey, A. Dalke, and K. Schulten, "VMD: Visual molecular dynamics," *Journal of Molecular Graphics*, vol. 14, no. 1, pp. 33–38, Feb. 1996, doi: 10.1016/0263-7855(96)00018-5.

[58] T. E. Oliphant, "Python for Scientific Computing," *Comput. Sci. Eng.*, vol. 9, no. 3, pp. 10–20, 2007, doi: 10.1109/MCSE.2007.58.

[59] M. Bauer, T. Schwarz-Selinger, W. Jacob, and A. von Keudell, "Growth precursors for a-C:H film deposition in pulsed inductively coupled methane plasmas," *Journal of Applied Physics*, vol. 98, no. 7, p. 073302, Oct. 2005, doi: 10.1063/1.2061890.

[60] M. Meier and A. von Keudell, "Hydrogen elimination as a key step for the formation of polymerlike hydrocarbon films," *Journal of Applied Physics*, vol. 90, no. 7, pp. 3585–3594, Oct. 2001, doi: 10.1063/1.1397285.

[61] A. von Keudell and W. Jacob, "Elementary processes in plasma–surface interaction: H-atom and ion-induced chemisorption of methyl on hydrocarbon film surfaces," *Progress in Surface Science*, vol. 76, no. 1–2, pp. 21–54, Sep. 2004, doi: 10.1016/j.progsurf.2004.05.001.

[62] C. Hopf, T. Schwarz-Selinger, W. Jacob, and A. von Keudell, "Surface loss probabilities of hydrocarbon radicals on amorphous hydrogenated carbon film surfaces," *Journal of Applied Physics*, vol. 87, no. 6, pp. 2719–2725, Mar. 2000, doi: 10.1063/1.372246.

[63] A. von Keudell, "Surface processes during thin-film growth," *Plasma Sources Sci. Technol.*, vol. 9, no. 4, pp. 455–467, Nov. 2000, doi: 10.1088/0963-0252/9/4/302.

[64] M. Sode, T. Schwarz-Selinger, W. Jacob, and H. Kersten, “Surface loss probability of atomic hydrogen for different electrode cover materials investigated in $H_2$-Ar low-pressure plasmas,” *Journal of Applied Physics*, vol. 116, no. 1, p. 013302, Jul. 2014, doi: 10.1063/1.4886123.

[65] M. Sode, W. Jacob, T. Schwarz-Selinger, and H. Kersten, “Measurement and modeling of neutral, radical, and ion densities in $H_2$-$N_2$-Ar plasmas,” *Journal of Applied Physics*, vol. 117, no. 8, p. 083303, Feb. 2015, doi: 10.1063/1.4913623.

[66] A. von Keudell, “Formation of polymer-like hydrocarbon films from radical beams of methyl and atomic hydrogen,” *Thin Solid Films*, vol. 402, no. 1–2, pp. 1–37, Jan. 2002, doi: 10.1016/S0040-6090(01)01670-4.

[67] W. M�ller, “Plasma and surface modeling of the deposition of hydrogenated carbon films from low-pressure methane plasmas,” *Appl. Phys. A*, vol. 56, no. 6, pp. 527–546, Jun. 1993, doi: 10.1007/BF00331402.

[68] A. von Keudell, T. Schwarz-Selinger, and W. Jacob, “Simultaneous interaction of methyl radicals and atomic hydrogen with amorphous hydrogenated carbon films,” *Journal of Applied Physics*, vol. 89, no. 5, pp. 2979–2986, Mar. 2001, doi: 10.1063/1.1343894.

[69] D. Hegemann, “Plasma activation mechanisms governed by specific energy input: Potential and perspectives,” *Plasma Processes & Polymers*, p. e2300010, Mar. 2023, doi: 10.1002/ppap.202300010.

[70] I. B. Denysenko *et al.*, “Modeling of argon–acetylene dusty plasma,” *Plasma Phys. Control. Fusion*, vol. 61, no. 1, p. 014014, Jan. 2019, doi: 10.1088/1361-6587/aade2d.

[71] C. De Bie, B. Verheyde, T. Martens, J. van Dijk, S. Paulussen, and A. Bogaerts, “Fluid Modeling of the Conversion of Methane into Higher Hydrocarbons in an Atmospheric Pressure Dielectric Barrier Discharge: Fluid Modeling of the Conversion of Methane …,” *Plasma Processes Polym.*, vol. 8, no. 11, pp. 1033–1058, Nov. 2011, doi: 10.1002/ppap.201100027.

[72] W. Bohmeyer *et al.*, “Transport and deposition of injected hydrocarbons in plasma generator PSI-2,” *Journal of Nuclear Materials*, vol. 337–339, pp. 89–93, Mar. 2005, doi: 10.1016/j.jnucmat.2004.10.107.

[73] V. De Vriendt, S. M. Miladinovic, J. L. Colaux, F. Maseri, C. L. Wilkins, and S. Lucas, “Growth Mechanisms Involved in the Synthesis of Smooth and Microtextured Films by Acetylene Magnetron Discharges,” *Langmuir*, vol. 27, no. 14, pp. 8913–8922, Jul. 2011, doi: 10.1021/la2003035.